aerospace

MDPI

Article

Wrapping Deployment Simulation Analysis of Leaf-Inspired Membrane Structures

Qiuhong Lin [1], Wenwen Jia [1], Huiying Wu [2], Ahmad B. H. Kueh [3], Yutao Wang [2], Kexin Wang [2] and Jianguo Cai [2,*]

[1] Beijing Institute of Spacecraft System Engineering, Beijing 100094, China; linqiuhong@buaa.edu.cn (Q.L.); 220140905@seu.edu.cn (W.J.)
[2] Key Laboratory of C & PC Structures of Ministry of Education, National Prestress Engineering Research Center, Southeast University, Nanjing 210096, China; 220201206@seu.edu.cn (H.W.); wangyutao@seu.edu.cn (Y.W.); 220171011@seu.edu.cn (K.W.)
[3] Department of Civil Engineering, Faculty of Engineering, Universiti Malaysia Sarawak, Kota Samarahan 94300, Sarawak, Malaysia; kbhahmad@unimas.my
* Correspondence: j.cai@seu.edu.cn

Abstract: Deployable membrane structures have received wide attention in many engineering applications, such as the military, aerospace, and aviation. Their properties of light weight and high storage ratio meet the requirements for aerospace exactly. In this paper, the wrapping deployment of membrane structures inspired by leaves are simulation-analyzed for prospective improvement. Three leaf-inspired patterns are investigated and discussed from the corresponding paper-craft design principles and deployment process perspectives. The deployment performance evaluation system according to the factors effecting working performance including maximum stress, driving force, maximum strain energy, smoothness index, and maximum folding height is established based on the results of the simulation analysis. Then, a comparison between the three patterns is carried out based on the deployment performance evaluation system. Moreover, it is found that adding creases reduces the folded height but the development performance gets worse. There is a balance between the folding ratio and development performance when the additional creases are added. The results can provide useful suggestions for designing wrapping deployment structures.

Keywords: wrapping deployment; origami; leaf-inspired membrane; deployment simulation

Citation: Lin, Q.; Jia, W.; Wu, H.; Kueh, A.B.H.; Wang, Y.; Wang, K.; Cai, J. Wrapping Deployment Simulation Analysis of Leaf-Inspired Membrane Structures. *Aerospace* **2021**, *8*, 218. https://doi.org/10.3390/aerospace8080218

Academic Editor: Igor Levchenko

Received: 8 July 2021
Accepted: 6 August 2021
Published: 8 August 2021

1. Introduction

Membrane structures make it possible for aerospace to apply large-scale components. In the realm of outer space exploration and applications, membrane structures have been used for solar sails [1–3], sun shields [4], and antennas [5,6]. Due to their ultra-low weight, small storage volume, and good performance in folding and deployment, membrane structures, particularly in their design and packaging have been an attractive focus in the field of space structure engineering for a long time [7,8].

To meet the high package ratio requirement, membrane structures have been designed based on origami. Origami is an ancient Asian paper-craft involving the folding of a flat sheet of paper into various forms without stretching, cutting, or gluing other pieces of paper to it. The Miura-ori pattern proposed by Koryo Miura [9] is the most classical origami. Its applicability is relevant to the design of structures like those found in Nature. For example, the deployment mechanisms of plant leaves from their early closed shape to their fully opened one can be ideally explained by origami models. Origami has been used in many fields [10–12]. Using this strategy, Focatiis and Guest [13] investigated a small strain mechanism of folding patterns through the inspiration of deploying tree leaves to produce polygonal foldable membranes as deployable structures.

At present, there is a great interest in achieving a high package ratio and efficient deployment in a vast diversity of applications. Wrapping folding is a great way to meet

these requirements, especially for membrane structures. A foldable annular sheet wrapping around a circular hub was invented by Scheel [14]. In the design, major creases were tangent to the hub, and the intermediate parts were additionally folded upon themselves between the major creases. Curved pleat folding was presented to package a square sheet around a central hub efficiently by Lee and Close [15]. Ishida et al. [16] employed conformal mapping and origami techniques to realize the systematic and efficient design of complex patterns based on simple ones. Compared with a flat membrane around a circular hub, Guest and Pellegrino [17] explored the alternative, non-symmetric foldable pattern wrapping around an n-sided polygon with straight sides. A rotationally skew folding membrane was examined by Furuya and Satou [18] to achieve the fully folding and compact storage of a spinning solar sail. Folding patterns of deployable structures based on some some basic geometrical considerations were also systematically presented. Segments were commonly folded for packaging in several manners, like z (zigzag) folding, roll-up folding, and telescopic folding [19].

One of the issues in membrane folding is the deviation of creases due to their thickness, so the thickness of the membrane has been a greatly studied parameter during the pattern design process. Satou and Furuya [20] examined the mechanical properties of a crease in the wrapping folding membrane to consider the effects of the folded thickness. The influence of membrane thickness and crease density on the driving force during the deployment of wrapping membrane structures was also investigated by Arya and Pellegrino [21]. The methods which considered thickness in the roll-up of the z foldingmembrane were proposed and classified by Sakamoto et al. [22], including two methods that kept the creases straight. The axis-shift and tapered panel methods were applied to add non-zero thickness to single-vertex multi-crease rigid origami to explore a feasible solution. Guang and Yang [23] identified the different geometrical characteristics of this kind of origami along this study line. Multiple spirals were used by Parque et al. [24] to form a new pattern to deploy flat and curved membranes with small thicknesses. Apart from these conceptual studies, wrapping membrane structures were investigated with the aid of physical models. By this approach, the integrity of the deployment mechanism was ensured in packaging and deploying membrane structures [25,26]. Overall, it is worth realizing that the field has adopted a diverse set of metrics, but there is a lack of specific indicators for evaluating the performance of the current folding schemes.

Because on-the-ground dynamic experiments of large membranes are difficult to perform and costly, numerical methods are essential to efficiently analyze the behaviors of membranes [27]. Numerical analysis promotes the deployment simulation of membrane structures in different fields of research. The spring-mass system was presented to perform numerical simulations of the centrifugal deployment technique by Okuizumi and Yamamoto [28]. The influence of different parameters on an inflatable membrane antenna was evaluated by Liu et al. [29] based on numerical simulations. Tessler et al. [30] adopted a geometrically nonlinear updated Lagrangian shell formulation in ABAQUS to simulate the formation of wrinkled deformations in membranes. Liyanage and Mallikarachchi [31] investigated the special characteristics of the deployment behavior for the two folding patterns of compact deployable structures by using the ABAQUS/Explicit software. Satou and Furuya [32] studied the deformed shape of the creased membrane to identify the dominant parameters and conditions of local buckling by the finite element method. A finite element modeling analysis was also used to interpret a multilayer membrane structure [33]. Cai et al. [34] studied the deployment behavior of Miura-ori structures by evaluating their maximum von Mises stress and smoothness index. Also, the effects of parametric changes during the deployment were considered. A finite element model was used by Wei et al. [35] to simulate the effects of membrane wrinkling for membrane precision engineering. Dynamic modeling for deploying the origami membrane structure considering contact-impact was executed by Yuan et al. [36]. Therefore, it is clear that by using the technology of the finite element software like ABAQUS, a dynamic simulation can be introduced to study the behaviors of wrapping membrane structures. Furthermore, the deployment simulation

results of membranes with different origami patterns can be investigated to choose an optimized origami pattern.

There are so many origami patterns of deployable membrane array structures, and it is difficult to evaluate them if there are no unified and effective indexes. The deployable membrane structures should be controlled to deploy smoothly before working in space, so it is important for membrane structures to deploy with low driving force and strain energy. Besides, for membrane structures, special membrane antenna, the requirement of their surface accuracy RMS is high and it directly affects their working performance. The smoothness of fully deployment plane membrane structures is relevant to the RMS. In this paper, three deployable origami patterns of a plane membrane surface inspired by leaves, like the sun shield membrane structure shown in Figure 1, are explored. The development processes are investigated and discussed by simulation analysis. Then, the deployment behaviors relevant to the working performance of each pattern, including driving force, maximum stress, strain energy, smoothness index, and folding height, are numerically obtained and assessed by ABAQUS. An optimal pattern is then obtained according to these behavioral indexes.

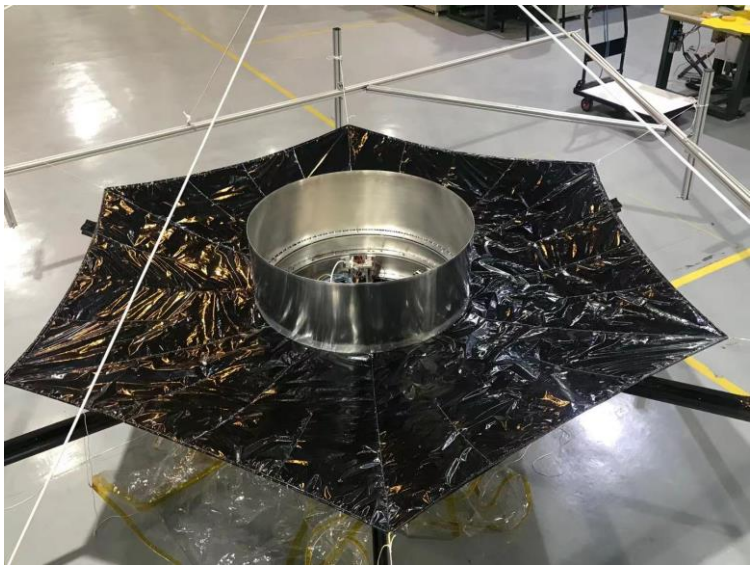

Figure 1. The model of a sun shield membrane.

2. The Deployment Patterns

2.1. The One-Leaf Unit

The development of the membrane structure is inspired by leaves. It has already been stated that origami models are a practical way to explain the process of unfolding of plant leaves from a closed shape to an open one. Several four–crease units for a single leaf can be formed. There are two folding methods for the one-leaf unit, as shown in Figure 2. Deployable membranes are composed of several leaf patterns around a hub. In the figure, solid lines and dashed lines indicate mountain creases and valley creases, respectively. Here, we denote further that the leaf-out pattern is the condition when the leaves along the midrib point outwards from the hub. The number of leaves in the pattern is n. The angles between the midrib and side veins are α_i, β_i ($i = 0,1 \ldots n$). The assumption about the geometrical angles defining the creases is given by:

$$\alpha_i = \beta_i, \tag{1}$$

The edges of the one-leaf unit are represented by a, b, c and d. According to the new folding pattern proposed by De Focatiis and Guest [10], the essential relationships of n and α_i are expressed as:

$$\alpha_i = \beta_i = \frac{\pi}{n},\ a \perp b,\ \ c \perp d,\ \ \ a = d,\ \ \ b = c, \tag{2}$$

Different from leaf-out, the leaves in the leaf-in pattern point along the midrib inwards from the hub. The corresponding relationships between n and α_i can be expressed as:

$$\alpha_i = \beta_i = \frac{\pi}{2} + \frac{\pi}{n},\ a \perp b,\ c \perp d,\ a = d,\ \ \ b = c, \tag{3}$$

(**a**) (**b**)

Figure 2. Two folding patterns of the one-leaf unit. (**a**) Leaf-out; (**b**) Leaf-in.

2.2. Candidate Deployment Patterns

Based on the assumption of zero thickness membrane, different deployable patterns, in which a flat membrane is wrapped around a central hub, are examined [9,37]. It is feasible to construct patterns like leaf-out and leaf-in to wrap around an n-sided polygon. The development in research and application has since discovered many different patterns from these premises. In order to systematically classify and summarize the plane wrapping origami membrane structures, a regular hexagon is selected as the central hub, and three typical patterns of a membrane structure are sorted out, as shown in Figure 3.

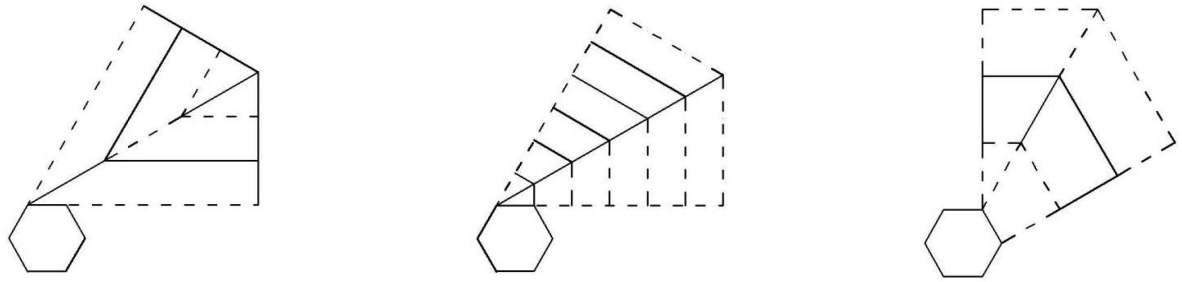

(**a**) (**b**) (**c**)

Figure 3. Three typical deployable patterns of the one-leaf unit around the hub. (**a**) Type 1; (**b**) Type 2; (**c**) Type 3.

Different designs are obtained by arranging the stems of leaves to meet at the hub at different sites. Figure 3a shows that the edges of the leaf-out unit are parallel and coincide with the hub edge. The angle between the midrib and the hub edge is 30°. In Figure 3b, the edges of the leaf-in unit are also parallel and coincide with the hub edge. The angle between the midrib and the hub edge is also 30°. Figure 3c illustrates that the midrib line of the leaf-in unit passes through the hub center point, and the angle between the midrib and the hub edge line is 60°. As shown in Figure 4 (17, 37), six identical one-leaf units can be assembled around a regular hexagon, and three patterns are obtained.

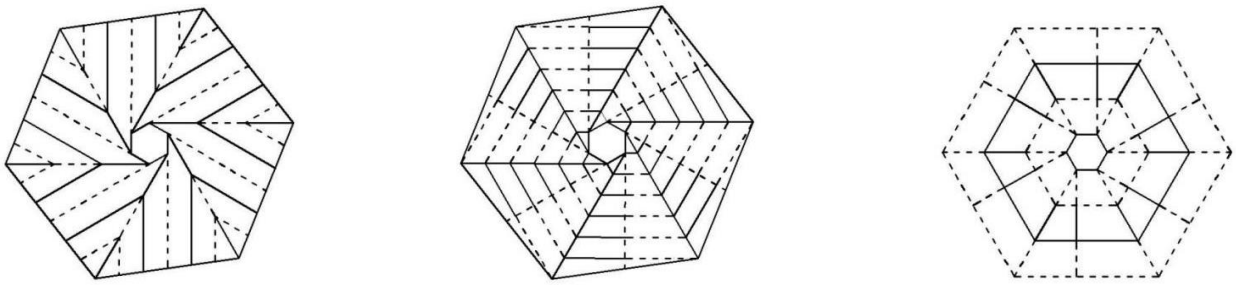

(**a**) (**b**) (**c**)

Figure 4. Three typical deployable patterns of plane wrapping origami membrane structures. (**a**) Pattern 1; (**b**) Pattern 2; (**c**) Pattern 3.

As shown in Figure 5, the folding process of Pattern 1 involves three motions. Each four-crease vertex of the midrib moves along the radial center, the midrib of the unit folds around the central hub, and the sectors wrap around the corners of the central polygon by additional creases. This deployable model can be extended to any regular polygon hub. The number of creases increases correspondingly with the number of sides of the regular polygon such that the folding of the membrane becomes smoother. However, deformation can be observed obviously near the hub, and wrinkles can also be seen on the deployed adjacent units. This results in the membrane being under tension in the state of complete folding, which may lead to damage along the sides of the regular polygon.

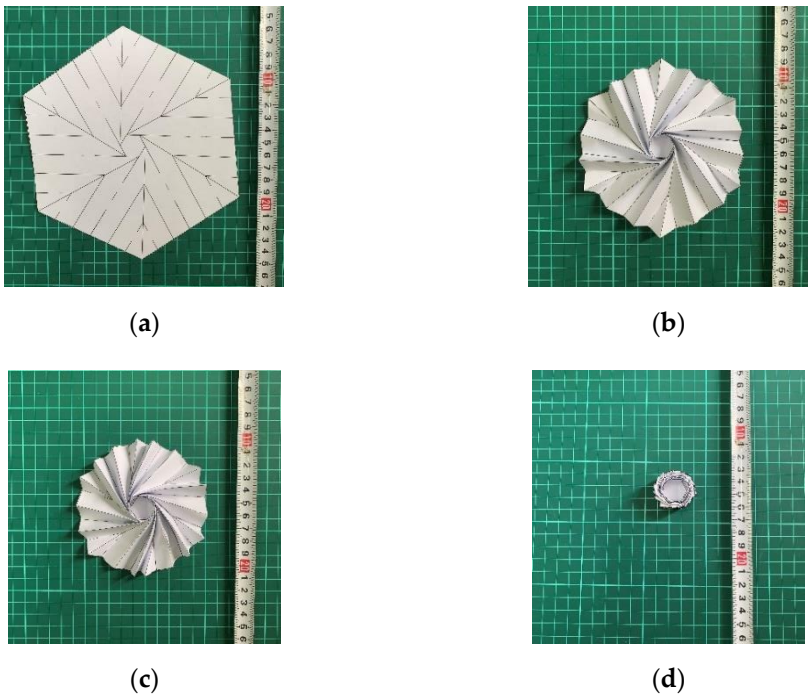

(**a**) (**b**)

(**c**) (**d**)

Figure 5. Folding sequences of the origami model of Pattern 1. (**a**) Completely deployed; (**b**) Folding process 1; (**c**) Folding process 2; (**d**) Completely folded.

According to the folding sequences shown in Figure 6, there are three motions in the deployment of Pattern 2. Firstly, there is a zigzag folding of the helix. A zigzag folding of the element edges parallel to the hub edges occurs simultaneously. Besides, there is the roll-up folding of the midrib around the central hub. The height of the leaves can be controlled by increasing or decreasing the number of creases.

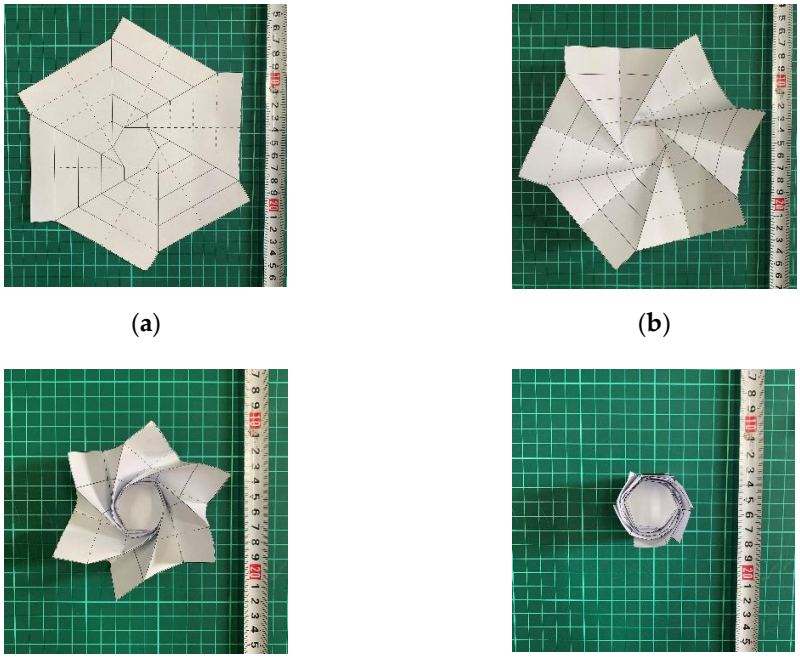

(**a**) (**b**)

(**c**) (**d**)

Figure 6. Folding sequences of the origami model of Pattern 2. (**a**) Completely deployed; (**b**) Folding process 1; (**c**) Folding process 2; (**d**) Completely folded.

As shown in Figure 7, there are three folding motions for Pattern 3: zfolding along the radial direction, roll-up folding along the circumferential direction, and wrapping of the arms around the central hub along the additional creases. The wrapping and folding processes are independent. However, folding deformation will occur at the creases of adjacent elements and the membrane at the center hub, with a further drawback of relatively large stress.

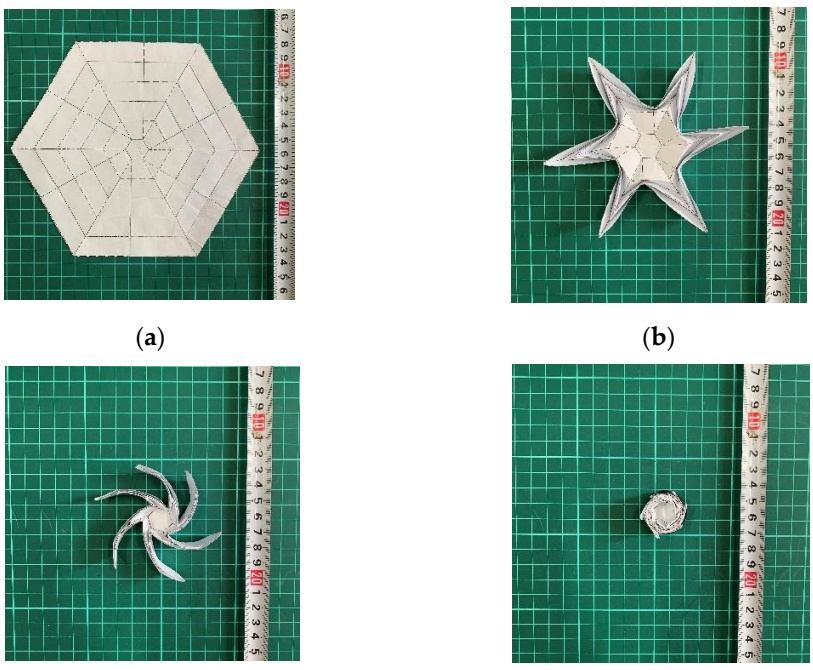

(**a**) (**b**)

(**c**) (**d**)

Figure 7. Folding sequences of the origami model of Pattern 3. (**a**) Completely deployed; (**b**) Folding process 1; (**c**) Folding process 2; (**d**) Completely folded.

3. Deployment Simulation of Wrapping Membrane Structures

3.1. Form-Finding

Since the shape of the membrane structure cannot be determined arbitrarily, it is necessary to seek the initial equilibrium surface shape that is suitable for the size and distribution of prestressing through form-finding. This process aims to ensure the conciliation of the deployable membrane structure with the equilibrium conditions while relying on certain pretension stress and flexural deformation to resist the external load of the membrane surface. If the initial stress and stress distribution are known and the surface geometry is taken as the solution target, the minimal surface method and the balanced surface method can be used to find the desired shape to meet the geometric boundary conditions. During the form-finding process, there is no change of the crease patterns. All that this process achieves is a scalloping of the outer perimeter of the membranes. The membranes are being subject to point tension loads at the outer corners of the membranes, and the form-finding method is attempting to avoid compressive loading by scalloping the edges. The plane wrapping origami membrane structures are set to an outer diameter of 5600 mm and an inner diameter of 800 mm. The relevant geometrical details of three patterns are shown in Figure 8.

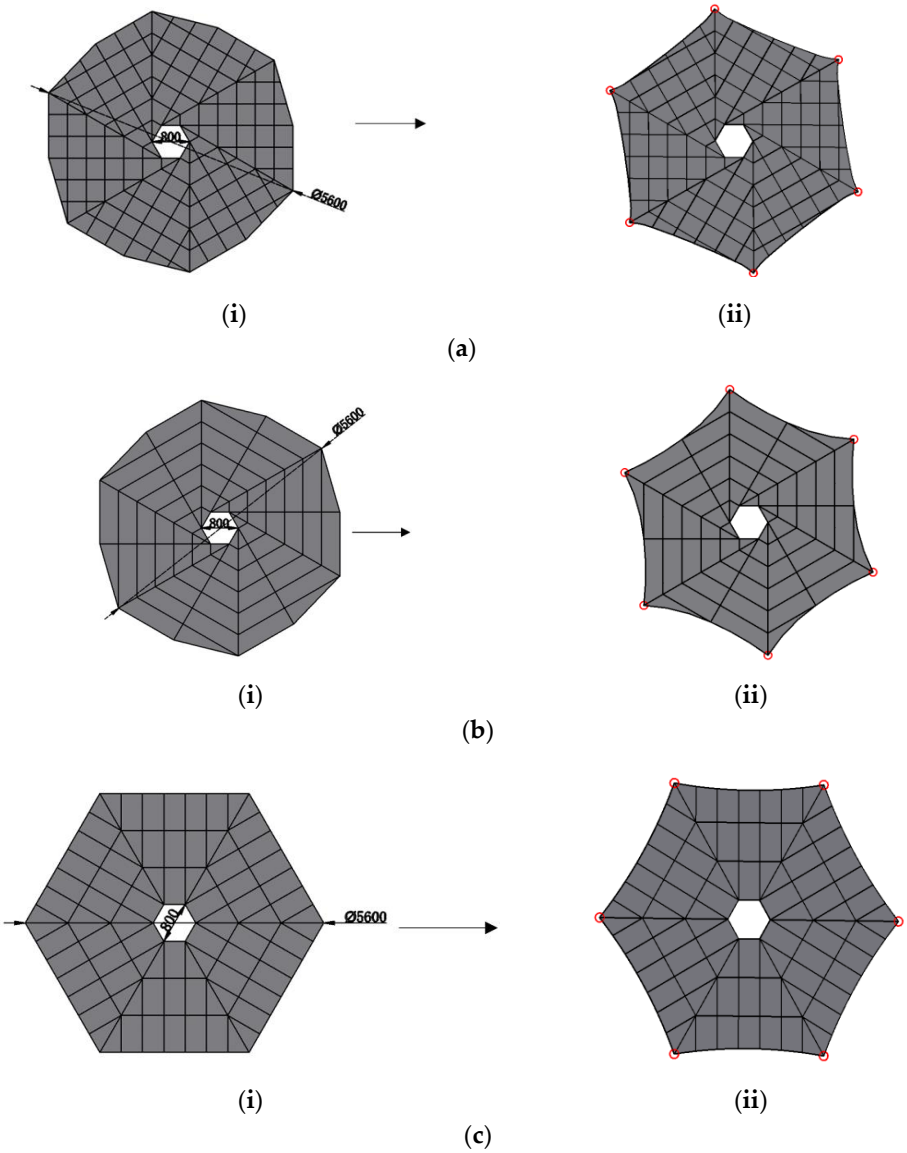

Figure 8. Form-finding of Patterns 1–3. (**a**) Pattern 1: (**i**) Before form-finding, (**ii**) After form-finding; (**b**) Pattern 2: (**i**) Before form-finding, (**ii**) After form-finding; (**c**) Pattern 3: (**i**) Before form-finding, (**ii**) After form-finding.

Firstly, the pretension stress of the membrane should be determined. Normally, the pretension stress of the membrane should be controlled to stay below 30% of the allowable stress, and the allowable stress of the membrane is about 25% of the ultimate uniaxial tensile strength of the membrane. In this paper, the membrane thickness is 0.05 mm, and the result from a preliminarily conducted test informs that the ultimate strength of the membrane is about 110 MPa. Thus, it can be determined that pretension stress should be below 9 MPa. In this paper, the pretension stress is the median value of 5 MPa. In the 3D3S software, the nonlinear finite element method is used to find the surface shape. According to the initial geometry assumed for the structure and the initial pretension set up in advance, the minimum or equilibrium surface of the membrane surface is solved iteratively.

When the initial geometric boundary conditions, initial stress value and distribution, and initial model shape are given, the pretension stress acting on the membrane is always kept unchanged during the iteration process. The minimal surface is found by the geometrically nonlinear finite element method. Once the equilibrium surface is found, the final shape finding of the pattern is achieved. The form-finding results of the three patterns are as illustrated in Figure 8.

3.2. Deployment Simulation

The deployment simulation is next performed with the following steps. First, 1/6 of the model is set to a fully folded state. A complete model can be established by a ring array. Second, the mesh is divided with a size of about 20 mm × 20 mm and there are about 13,800 elements of each model. The thickness of the membrane is prescribed as 0.05 mm, the elastic modulus is 2400 MPa, and the Poisson's ratio is 0.38. Element types M3D4R and M3D3 are selected as membrane elements for quadrilateral mesh and triangular mesh, respectively. For the loadings, they drive the membrane structures to deploy, so they are on the most outer edge. For convenience to set the loadings, the local cylindrical coordinate system has been established. The driving loading velocity is 10 mm/s in V1 in the local cylindrical coordinate system. The locations of six driving loadings are marked with red circles in fully deployed state. About the constraints boundary of models, the displacements of the nodes on inner edges are restricted to U1 = U2 = U3 = 0. A dynamic explicit analysis step is adopted. The locations of constraints and loadings on the FE models are shown in Figure 9.

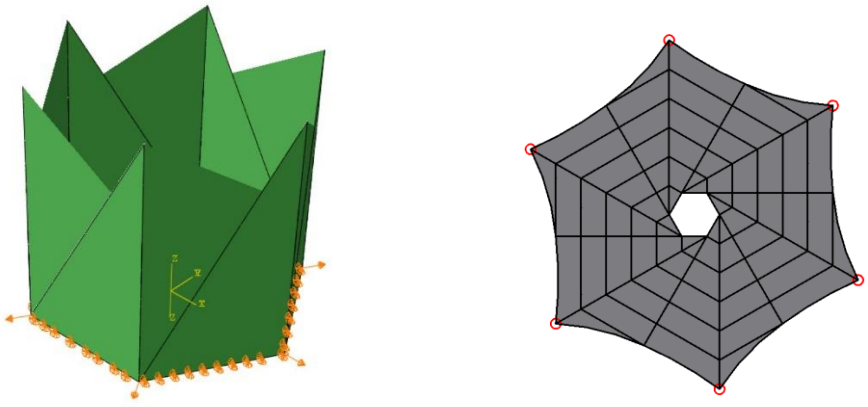

(**a**) (**b**)

Figure 9. Locations of constraints and loadings on the FE model. (**a**) Fully folded state (**b**) Fully deployed state.

There are two main assumptions in the FE models. Firstly, the property of the material is ideal elastic material and exists no plastic deformation. The membrane material commonly uses polyimide film material and its strength is more than 100 MPa. In this paper, the

stresses of membrane structures in the whole deployment phase are kept under 100 MPa, so the material is in elastic phase. Secondly, the loadings are acting on the nodes and there is stress concentration. During the actual operation, each driving loading is acting on an area and the stress distribution became more even. This design is even more detrimental to the FE models performed in this paper. However, the area effected by stress concentration is small. In this paper, the elements near the loading points are removed, and the elements are covered by the circles with the loading point as the center and 0.08 m as the radius, so the above assumptions are reasonable. In addition, we have done a deployment test for a membrane structure of pattern 3 as shown in Figure 1. The membrane structure deployed smoothly during the whole process, so we can conclude that the FE models are rational. The stress contour plot of the three patterns after form-finding during the deployment process are shown in Figures 10–12.

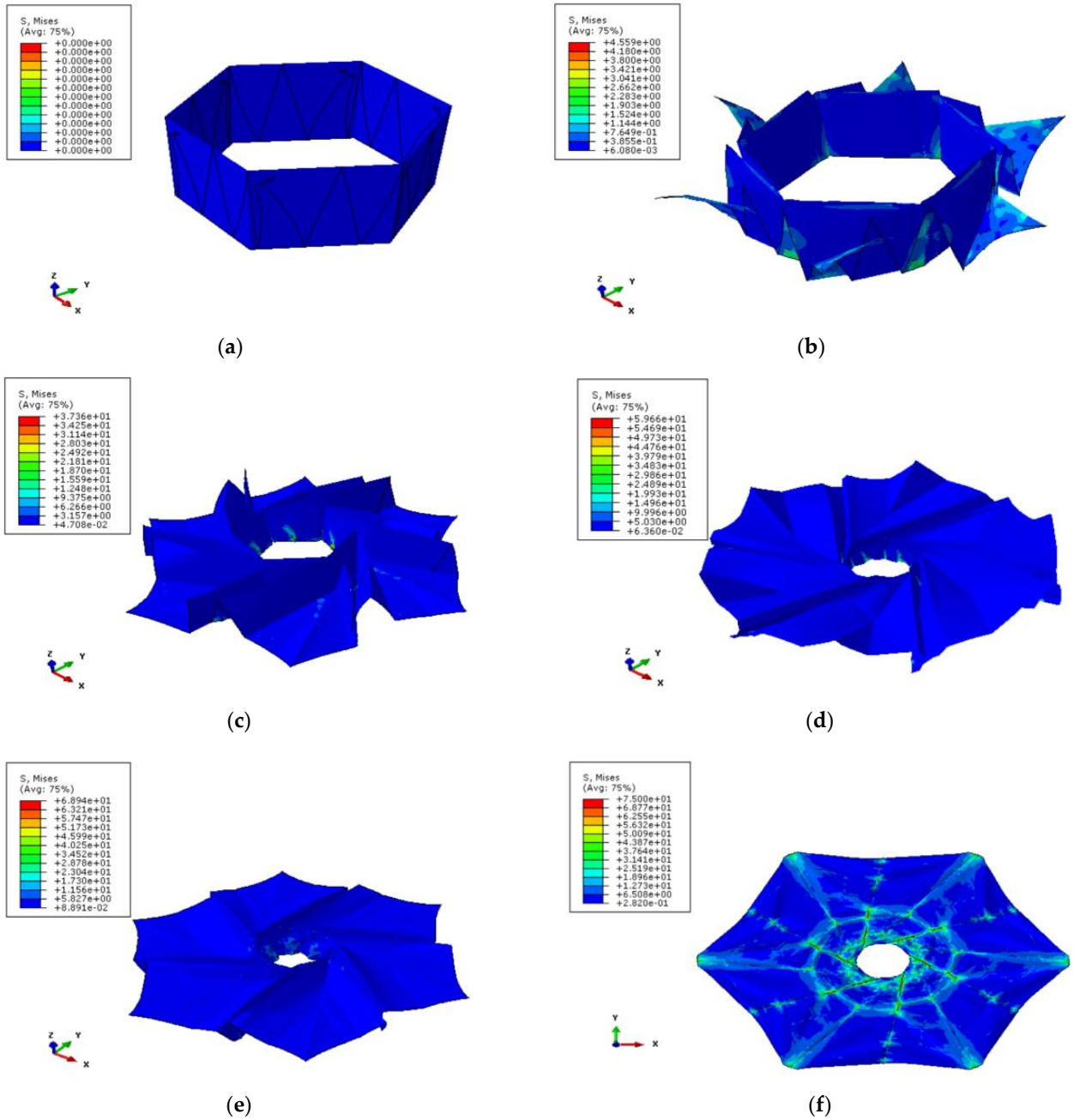

Figure 10. Stress contour plot of Pattern 1 during deployment (MPa). (**a**) Fully folded state; (**b**) 10% deployment; (**c**) 30% deployment; (**d**) 50% deployment; (**e**) 70% deployment; (**f**) 100% deployment.

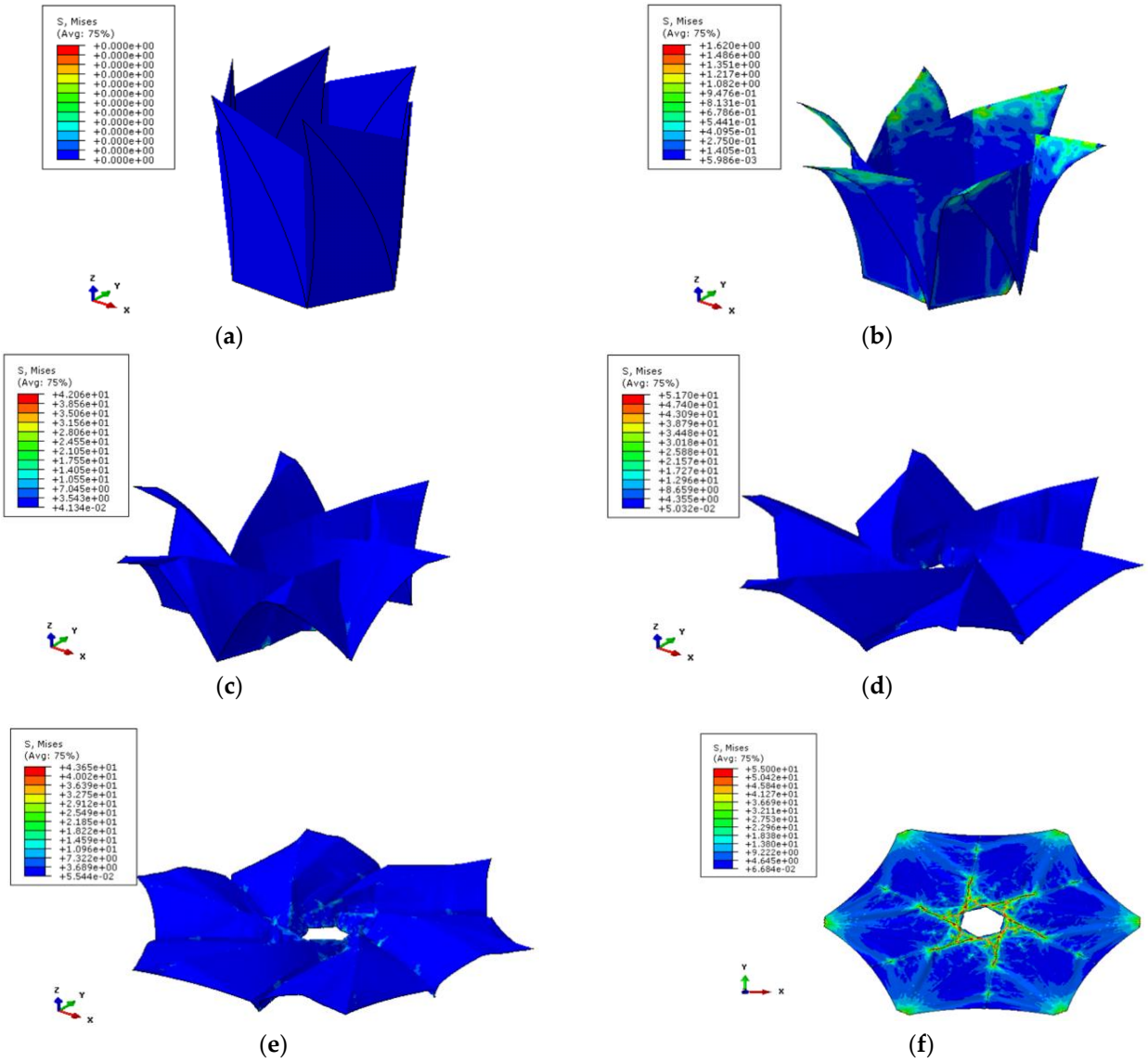

Figure 11. Stress contour plot of Pattern 2 during deployment (MPa). (**a**) Fully folded state; (**b**) 10% deployment; (**c**) 30% deployment; (**d**) 50% deployment; (**e**) 70% deployment; (**f**) 100% deployment.

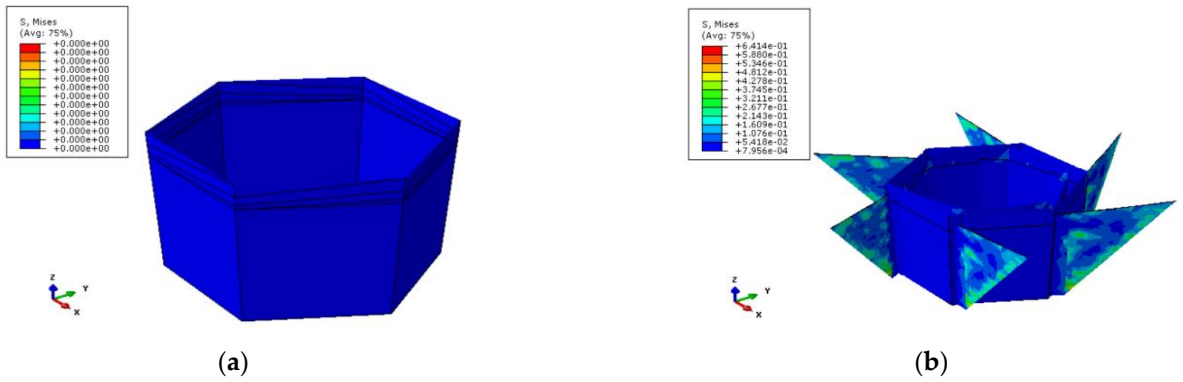

Figure 12. *Cont.*

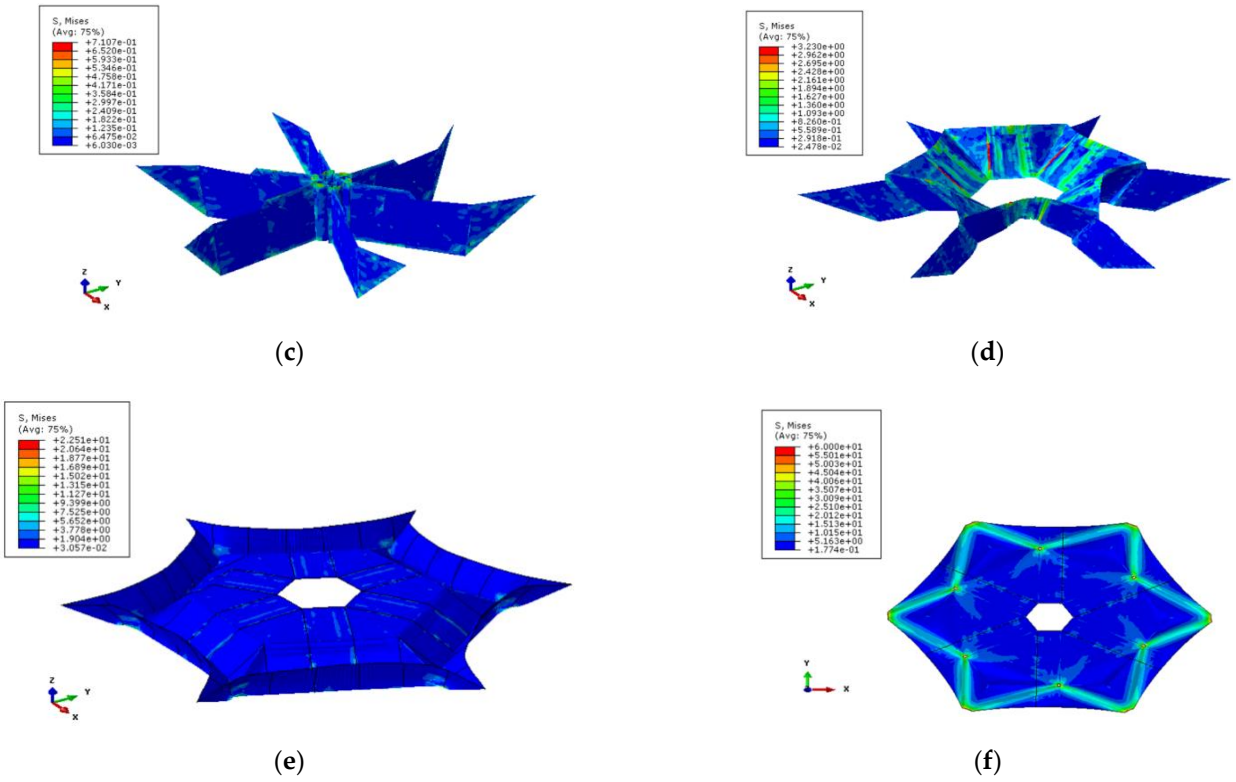

Figure 12. Stress contour plot of Pattern 3 during deployment (MPa). (**a**) Fully folded state; (**b**) 10% deployment; (**c**) 30% deployment; (**d**) 50% deployment; (**e**) 70% deployment; (**f**) 100% deployment.

3.3. Deployment Responses

For the requirement of working performance, the maximum stress, driving force, strain energy, and smoothness during the deploying process should be analyzed and controlled. In the simulation, the maximum stress, driving force, strain energy, and smoothness index of the deploying process as unified and effective indexes are examined to evaluate the deployment performance. Due to the relatively large stress at the loading point of all the three folding patterns, a remedial treatment will be carried out in the actual engineering. Therefore, in the fully deployed stress contour plot, the elements near the loading points can be removed, and the elements are covered by the circles with the loading point as the center and 0.08 m as the radius, as shown in Figure 8. The different maximum stress histories evolution of the three considered patterns are illustrated in Figure 13. The stress increases with deployment, and the maximum stress of Patterns 1, 2, and 3 are 75 MPa, 55 MPa, and 60 MPa, respectively.

For Pattern 1, the maximum stress of the structure is low when it is at the initial stage of deployment, with a somewhat high growth rate during 0~0.4 s. After that, the growth rate of the maximum stress of the inner structure slows down. Finally, the membrane has been deployed into a flat state, which reduces its growth rate markedly. There is a different trend for the maximum stress for Pattern 2. Before 0.4 s, the maximum stress of the structure is similar to Pattern 1. However, the stress decreases suddenly in 0.4~0.7 s, which indicates that the deformation decreases sharply in the process from unwrapping to deployment. Besides, there is a plateau for the maximum stress after 0.8 s. For Pattern 3, the maximum stress of the structure is almost zero within 0~0.4 s, which indicates the rigid displacement is dominant, and a litter deformation occurs in the membrane. After 0.4~0.6 s, the maximum stress of the structure begins to increase slightly. Since the interaction and coupling effects between elements are very high, the maximum stress rises sharply after 0.7 s.

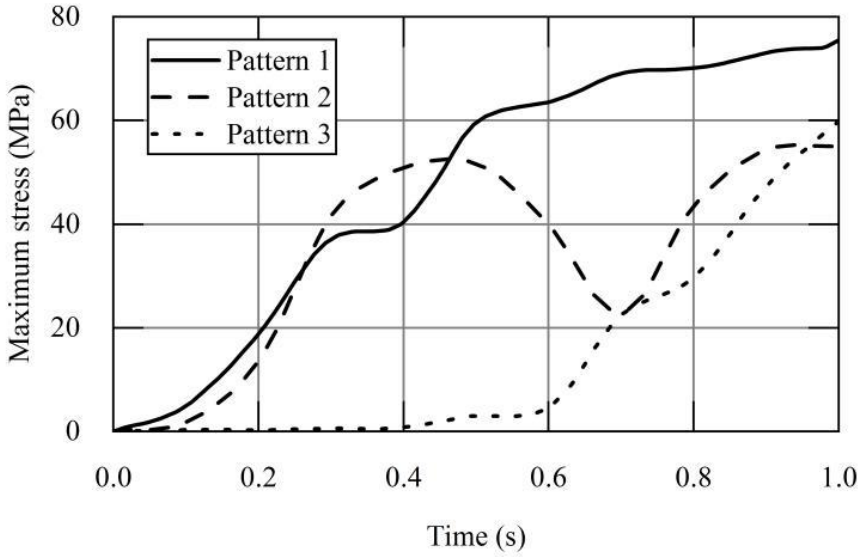

Figure 13. Maximum stress-time curves of the three patterns during deployment.

At the beginning of the deployment, the magnitude of the driving force is very small, as shown in Figure 14. To ensure the smoothness of the model after deployment, the displacement load exceeds the actual size, thus causing the models to experience the "over-tension" state. The driving force suddenly will spike after the over-tension state, which corresponds to the working states with initial prestress. In Patterns 1, 2, and 3, the maximum driving forces before over-tension are 5.22 N, 1.51 N, and 0.28 N, respectively.

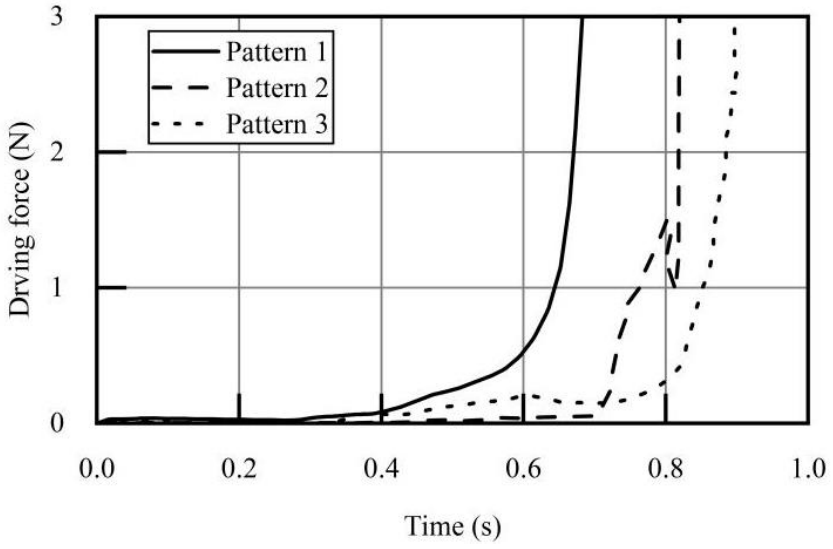

Figure 14. Driving force-time curves of the three patterns during deployment.

It can be seen from Figure 15 that the energy growth curves of the three folding patterns have no obvious oscillation phenomena, and they are always in the small range. Before 0.8 s, the deformation energy is very small. The subsequent increment is minor with respect to the loading time, which indicates that the membrane has almost no deformation at the beginning of the deployment. The energy increases significantly after 0.8 s, which corresponds to the peaking of the first principal stress. At this point, the whole structure begins to undergo a large elastic deformation. The deformation increases further due to over-tension, though it is within the allowable deformation range of the material. It is noticed that the ratio of kinetic energy to internal energy is always less than 5%, which

conforms to the quasi-static response, therefore ensuring the reliability of the computed results and the stability of the deployment.

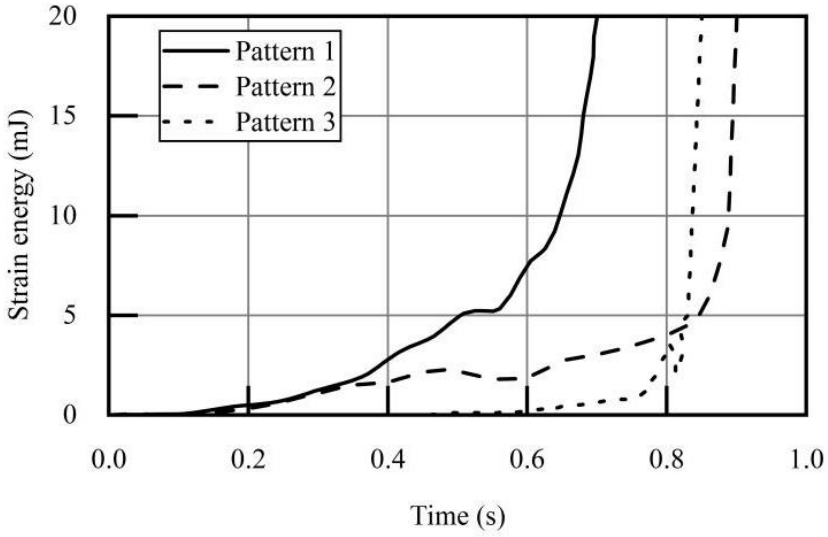

Figure 15. Strain energy-time curves of the three patterns during deployment.

When calculating the model smoothness index, it is necessary to determine the ideal plane at first (datum), because the displacement of the loading point is determined by the difference between the coordinates of the initial state and those of the ideally expanded. Since the loading point is located on the ideal plane, the coordinates of the three desired points can be found from the loading points for the ideal plane. Then, the distance difference from the ideal plane is calculated by using the coordinates of other points on the model. Finally, the smoothness index, P, can be attained by computing the root mean square of all points:

$$P = \sqrt{\frac{1}{j}\sum_{i=1}^{j} p_i^2} = \sqrt{\frac{p_1^2 + p_2^2 + \cdots + p_j^2}{j}}, \quad (4)$$

where j is the total node number, and P_i is the distance from node i to the ideal plane. For the structural settings illustrated in Figures 9f, 10f and 11f, the coordinates for the 3 corner nodes are summarized in Table 1. A, B, C are the three loading points of the thin membrane driving position. The equations of the plane defined by these three nodes are also given. The smoothness indexes of the folded patterns are 1.348618 mm, 0.95647 mm, and 1.0080 mm, respectively.

Table 1. Coordinates of nodes A, B, and C (mm).

Pattern	Coordinate	A	B	C	Equation of Idea Planes
Pattern 1	X	−59.751	−45.048	−41.672	120.86 z-2752.02 = 0
	Y	146.414	162.394	157.843	
	Z	22.770	22.770	22.770	
Pattern 2	X	−70.9675	−40.9819	−28.8771	480.35 z-21,884.55 = 0
	Y	154.728	150.593	164.943	
	Z	45.5599	45.5599	45.5599	
Pattern 3	X	137.304	137.235	138.985	5.85 z-195.40 = 0
	Y	−210.955	−213.832	−225.654	
	Z	33.3995	33.3995	33.3712	

From the comprehensive analysis of the deploying process for the three patterns, it can be found in Table 2 that the maximum stress, maximum driving force, and maximum strain energy of Pattern 2 are all small. Also, at the same loading time and loading point, the smoothness of Pattern 2 is the best; because its folding mode is simple, the folding times are the least, its wrinkles are relatively less, and it is easier to develop into a plane. Moreover, it is observed that its corresponding deformation is small and the creases are comparatively lesser. However, the disadvantage of Pattern 2 is that its height after folding is higher than the other patterns, which is not conducive to the requirement of storage. Therefore, appropriate creases will be considered to reduce its folded height next.

Table 2. Comparison of chief results of the three folding patterns.

Pattern	Maximum Stress (MPa)	Maximum Driving Force (N)	Maximum Strain Energy (mJ)	Smoothness Index (mm)	Folding Height (cm)
Pattern 1	75	5.22	19.81	1.49	46.19
Pattern 2	55	0.28	4.18	0.96	138.56
Pattern 3	60	1.51	3.35	1.01	69.28

4. Crease Optimization Strategy

4.1. Creases Distribution

It can be found that the folding height of Pattern 2 is higher, so the optimization strategy for the crease distribution is proposed [38]. The inner and outer diameters remain unchanged as 800 mm and 5600 mm, respectively. The addition of creases is considered to reduce the folded height to achieve a higher package ratio. The proposed distributions of creases are shown in Figure 16. The additional creases in 1/6 of model are perpendicular to the original creases. There are two additional creases in pattern 2a and four additional creases in pattern 2b. The more additional creases it adds, the higher the package ratio is. However, the additional creases may cause the increase of stress during the deployment, so the optimized design for additional creases should be considered.

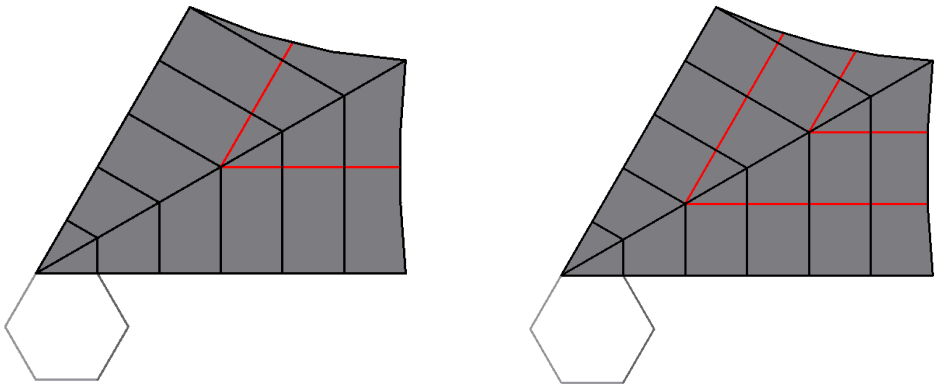

(**a**) (**b**)

Figure 16. Schematic diagram of two different variants of Pattern 2. (**a**) Pattern 2a: Adding two creases; (**b**) Pattern 2b: Adding four creases.

4.2. Deployment Performance

The deployment processes of membrane with proposed creases distributions can be found in Figures 17 and 18. Additional creases perpendicular to the axial bending crease are added to the diagonal crease, which reduces the height after folding. The membranes are initially wound around the hexagonal central hub and gradually deployed along the wrapping direction. A larger stress is still noticed at the loading points and the crease after the final, full deployment. Compared with the original Pattern 2 model without additional creases, the maximum stress has increased due to the stress mutation at the vertexes from

the folding state to that of deployed. The stress concentration is easily formed at the creases convergence point after full deployment.

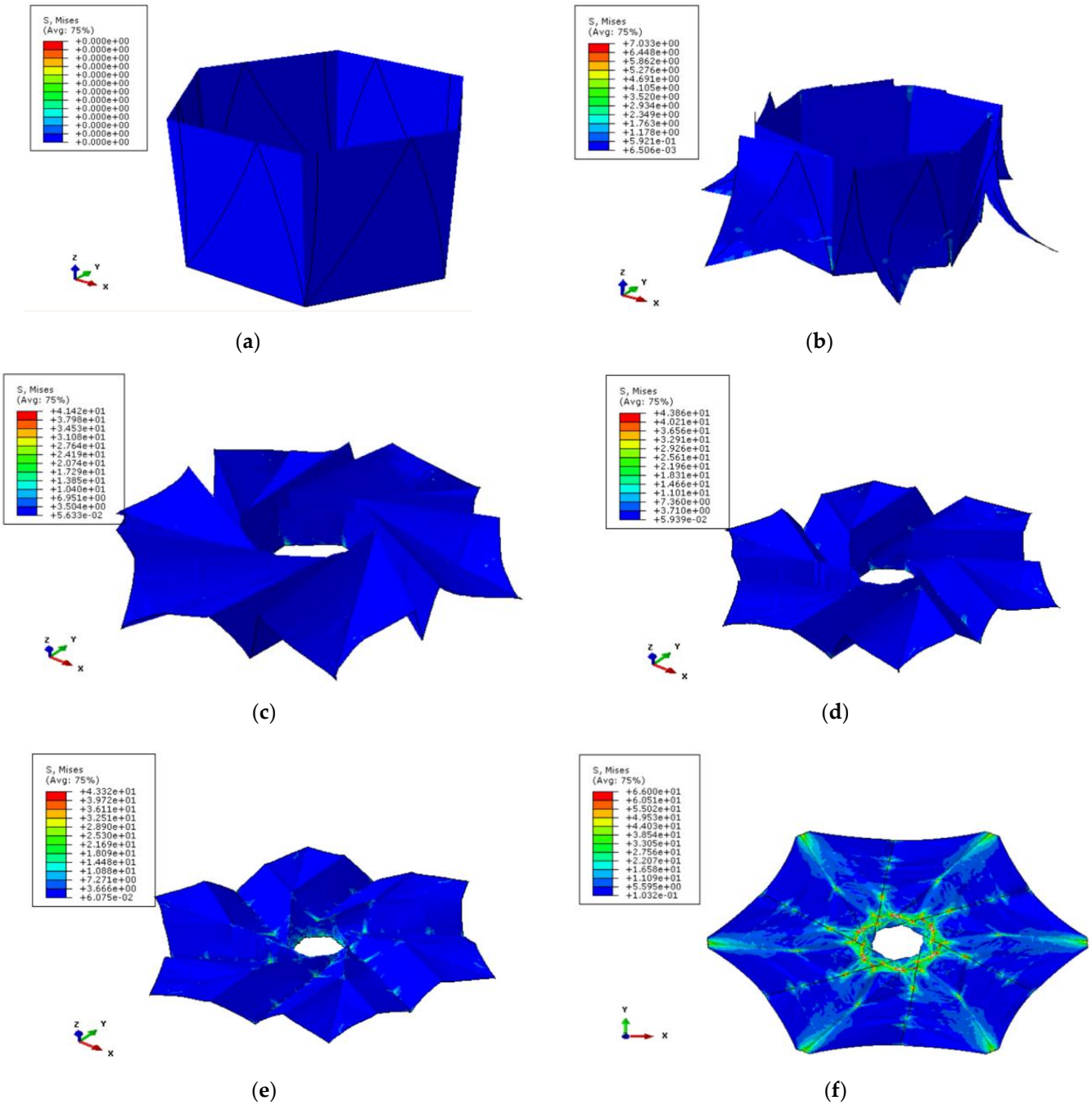

Figure 17. Stress contour diagram of the deploying process of Patterns 2a (MPa). (**a**) Fully folded state; (**b**) 10% deployment; (**c**) 30% deployment; (**d**) 50% deployment; (**e**) 70% deployment; (**f**) 100% deployment.

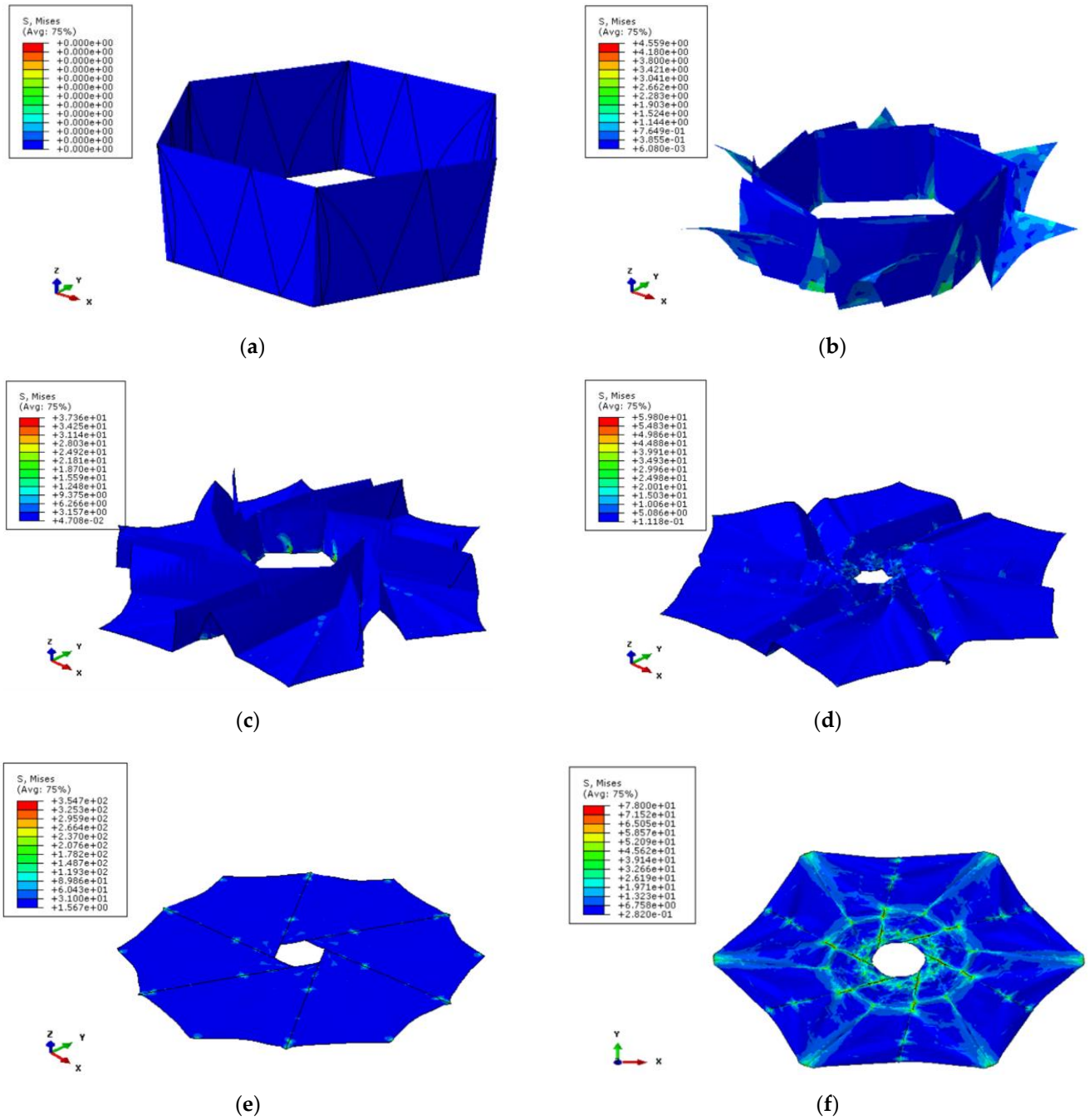

Figure 18. Stress contour diagram of the deploying process of Patterns 2b (MPa). (**a**) Fully folded state; (**b**) 10% deployment; (**c**) 30% deployment; (**d**) 50% deployment; (**e**) 70% deployment; (**f**) 100% deployment.

It can be seen from Figure 19 that the maximum stresses of the two modified patterns are low during 0~0.6 s. The deploying process is dominated by rigid displacement, and the stress growth is relatively gradual. After 0.6 s, the structures steadily enter the elastic deformation stage, during which the maximum stress begins to increase significantly. The maximum stresses peak at 1.0 s, about 66 MPa and 78 MPa for adding two and four creases, respectively.

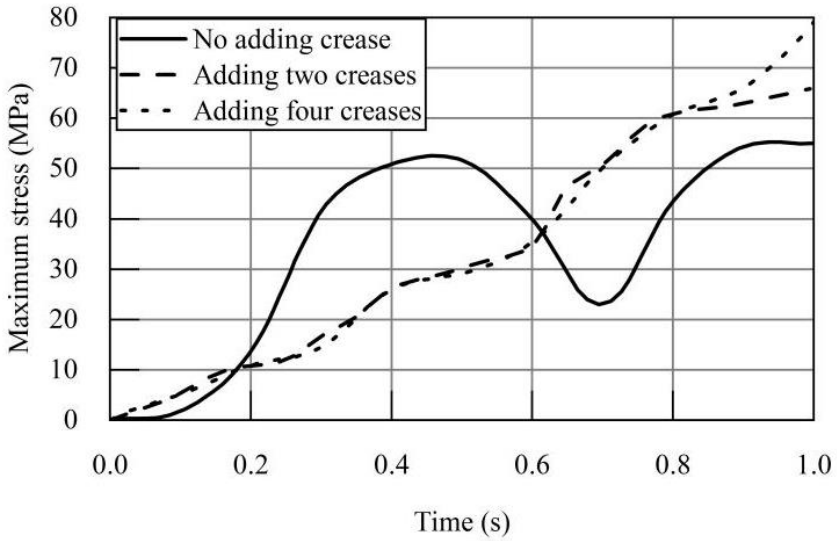

Figure 19. Maximum stress-time curves of the new two patterns during deployment.

The driving forces of the two modified models are very small during the entire deploying sequence, as shown in Figure 20. The maximum forces of the models in the cases of adding two and four creases before over-tension are 0.29 N and 0.33 N, respectively. Even though the driving forces are larger than that of Pattern 3, it is still ideal for deployment. It can be seen from Figure 21 that the overall strain energy levels of the models due to adding two and four creases remain very small before over-tensioning occurs. The changing trend of the strain energy of these two models is similar to that of the original Pattern 2. The maximum strain energy before over-tension is larger than that of the original Pattern 2, but the increment is very small. It is still considered as a low energy-driven deployment. Based on the coordinates of the 3 corner nodes listed in Table 3, the smoothness indexes of the folding patterns are 0.96 mm, 1.20 mm, and 1.49 mm, respectively. The smoothness decreases with the increase of the number of additional creases.

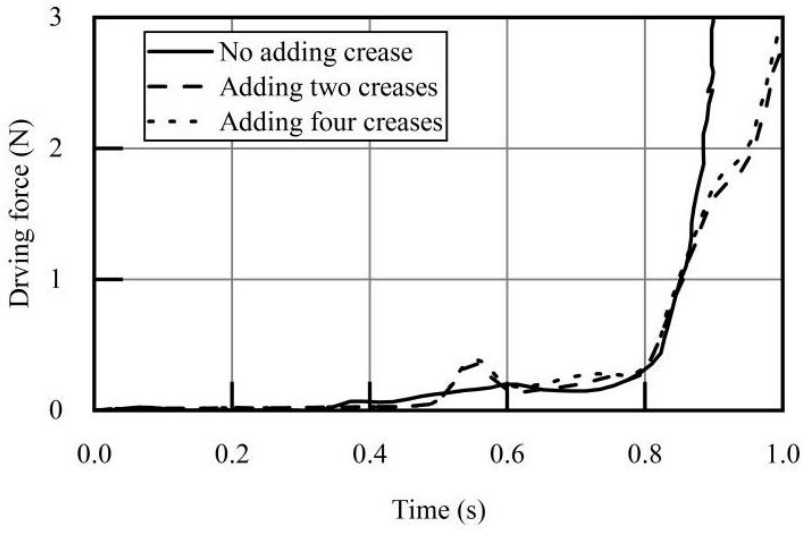

Figure 20. Driving force-time curves of the new two patterns during deployment.

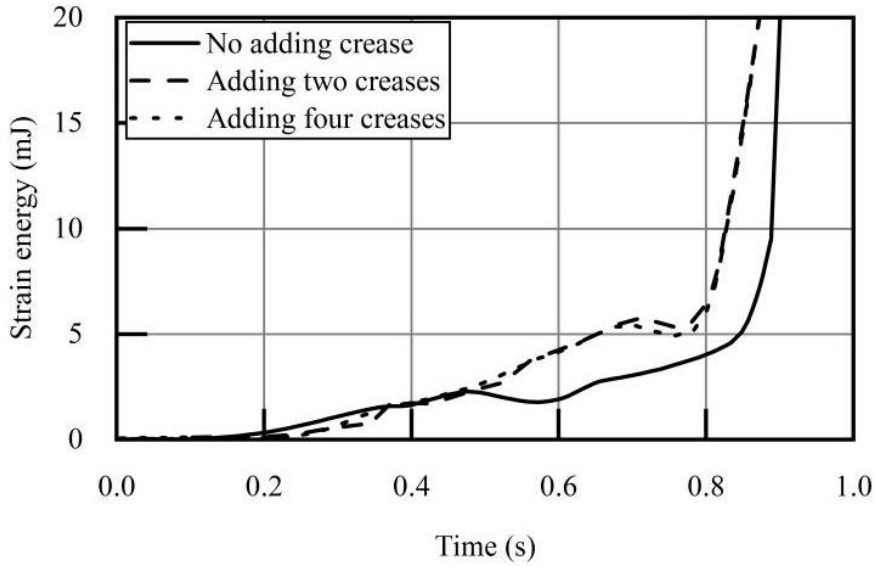

Figure 21. Strain energy-time curves of the new two patterns during deployment.

Table 3. Coordinates of nodes A, B, and C (mm).

Pattern	Coordinate	A	B	C
Pattern 2a	X	94.3535	92.3292	90.1491
	Y	40.4019	42.3878	46.1852
	Z	50.4973	50.4973	50.4973
Pattern 2b	X	50.6343	42.6613	30.7569
	Y	66.5513	80.6865	73.4856
	Z	31.2555	31.2555	31.2555

The comparison between the development performances of Patterns 2, 2a and 2b is given in Table 4. With the increase in the number of additional creases, the folded heights decrease by 49.95% and 66.66% for two and four additional creases, respectively. The corresponding folded ratio increases. However, there is a little increase in the maximum stress, maximum driving force, maximum strain energy and smoothness index. The cost will go up in the deploying process, so there is a balance between the folded package ratio and the deployed performance.

Table 4. Comparison of development performance for Pattern 2 and its variants.

Pattern	Maximum Stress (MPa)	Maximum Driving Force (N)	Maximum Strain Energy (mJ)	Smoothness Index (mm)	Folding Height (cm)
Pattern 2	55	0.28	4.18	0.96	138.56
Pattern 2a	66	0.30	5.86	1.20	69.39
Pattern 2b	78	0.33	6.38	1.49	46.19

5. Conclusions

In this paper, the development of three leaves-inspired patterns of plane wrapping origami membrane structures are numerically investigated. Their deployment behavior characteristics relevant to the working performance, including maximum stress, driving force, smoothness index, and strain energy, are systematically compared. Among the studied patterns, Pattern 2 meets the performance requirement best in terms of attaining low stress, driving force, and strain energy with the best smoothness index. Attributable to a simple folding mode, it is easier to develop into a plane. In order to reduce the folding height of Pattern 2, extra creases are added, but it is detrimental for the development

process. There is a balance between the folded package ratio and development performance, which corresponds to the storage state and the development state, respectively. Moreover, the effects of loading time, edge cables and other development parameters are not considered in this work, but should be discussed in the future.

Author Contributions: Conceptualization, J.C. and Q.L.; methodology, W.J. and Y.W.; software, K.W. and H.W.; validation, Q.L., Y.W. and J.C.; formal analysis, K.W. and Y.W.; investigation, H.W. and Y.W.; resources, Q.L.; data curation, W.J.; writing—original draft preparation, K.W. and H.W.; writing—review and editing, A.B.H.K., Y.W. and J.C.; visualization, W.J.; supervision, J.C.; project administration, J.C.; funding acquisition, Q.L. and J.C. All authors have read and agreed to the published version of the manuscript.

Funding: This research was funded by THE NATIONAL NATURAL SCIENCE FOUNDATION OF CHINA, grant number 51822805, 51878147 and U1937202 and CIVIL AEROSPACE TECHNOLOGY RESEARCH PROJECT, grant number D030202.

Conflicts of Interest: The authors declare no conflict of interest.

References

1. Leipold, M.; Eiden, M.; Gamer, C.E.; Herbeck, L.; Kassing, D.; Niederstadt, T.; Kruger, T.; Pagel, G.; Rezazad, M.; Rozemeijer, H.; et al. Solar sail technology development and demonstration. *Acta Astronaut.* **2003**, *52*, 317–326. [CrossRef]
2. Sawada, H.; Shirasawa, Y.; Mori, O.; Okuizumi, N.; Miyazaki, Y.; Matunaga, S.; Furuya, H.; Sakamoto, H.; Natori, M.; Tsuda, Y. On-orbit result and analysis of sail deployment of world's first solar power sail IKAROS. *J. Space Technol. Sci.* **2013**, *27*, 54–68. [CrossRef]
3. Seefeldt, P.; Spietz, P.; Sproewitz, T.; Grundmann, J.T.; Hillebrandt, M.; Hobbie, C.; Ruffer, M.; Straubel, M.; Toth, N.; Zander, M. Gossamer-1: Mission concept and technology for a controlled deployment of gossamer spacecraft. *Adv. Space Res.* **2017**, *59*, 434–456. [CrossRef]
4. Johnston, J.D.; Ross, B.D.; Blandino, J.; Lawrence, J.; Perrygo, C.M. Development of sunshield structures for large space telescopes. *Proc. SPIE Int. Soc. Opt. Eng.* **2003**, *4850*, 209–220. [CrossRef]
5. Wang, Y.; Liu, R.; Yang, H. Design and deployment analysis of modular deployable structure for large antennas. *J. Spacecr. Rockets* **2015**, *52*, 1101–1111. [CrossRef]
6. Liu, C.; Shi, Y.Y. Comprehensive structural analysis and optimization of the electrostatic forming membrane reflector deployable antenna. *Aerosp. Sci. Technol.* **2016**, *53*, 267–279. [CrossRef]
7. Hu, J.H.; Chen, W.J.; Qu, Y.G.; Yang, D.Q. Safety and serviceability of membrane buildings: A critical review on architectural, material and structural performance. *Eng. Struct.* **2020**, *210*, 110292. [CrossRef]
8. Tao, Q.; Wang, C.G.; Wang, K.; Tan, H.F. Mixed triangle lattice reinforced membrane antenna reflector: Design and analysis. *AIAA J.* **2020**, *58*, 1897–1900. [CrossRef]
9. Miura, K. Method of packaging and deployment of large membranes in space. In Proceedings of the 31st Congress of International Astronautical Federation, Tokyo, Japan, 21–28 September 1980.
10. Zhou, Y.; Zhang, Q.; Cai, J.G.; Zhang, Y.T.; Feng, J. Experimental study of the hysteretic behavior of energy dissipation braces based on Miura origami. *Thin Walled Struct.* **2021**, *167*, 108196. [CrossRef]
11. Zhang, Q.; Pan, N.; Meloni, M.; Lu, D.; Feng, J. Reliability Analysis of Radially Retractable Roofs with Revolute Joint Clearances. Reliability Engineering. *Syst. Saf.* **2020**, *208*, 107401. [CrossRef]
12. Meloni, M.; Cai, J.G.; Zhang, Q.; Sang-Hoon, D.; Li, M.; Ma, R.J.; Parashkevov, T.E.; Feng, J. Engineering Origami: A Comprehensive Review of Recent Applications, Design Methods, and Tools. *Adv. Sci.* **2021**, *8*, 2000636. [CrossRef]
13. Focatiis, D.S.A.D.; Guest, S.D. Deployable membranes designed from folding tree leaves. *Phil. Trans. R. Soc. A* **2002**, *360*, 227–238. [CrossRef] [PubMed]
14. Scheel, H. Space-Saving Storage of Flexible Sheets. U.S. Patent 3,848,821, 19 November 1974.
15. Lee, N.; Close, S. Curved pleat folding for smooth wrapping. *Proc. R. Soc. A Math. Phys.* **2013**, *469*, 20130152. [CrossRef]
16. Ishida, S.; Nojima, T.; Hagiwara, I. Design of deployable membranes using conformal mapping. *J. Mech. Design.* **2015**, *137*, 061404. [CrossRef]
17. Guest, S.D.; Pellegrino, S. Inextensional wrapping of flat membranes. Structural Morphology. In Proceedings of the First International Seminar on Structural Morphology, Montpellier, France, 11 September 1992; pp. 203–215.
18. Furuya, H.; Satou, Y. Deployment and retraction mechanisms for spinning solar sail membrane. In Proceedings of the 49th AIAA/ASME/ASCE/AHS/ASC Structures, Structural Dynamics, and Materials Conference, Schaumburg, IL, USA, 7–10 April 2008; pp. 1–11.
19. Natori, M.C.; Sakamoto, H.; Katsumata, N.; Yamakawa, H.; Kishimoto, N. Conceptual model study using origami for membrane space structures—A perspective of origami-based engineering. *Mech. Eng. Rev.* **2015**, *2*, 1–15. [CrossRef]

20. Satou, Y.; Furuya, H. Fold line based on mechanical properties of crease in wrapping fold membrane. In Proceedings of the 54th AIAA/ASME/ASCE/AHS/ASC Structures, Structural Dynamics, and Materials Conference, Boston, MA, USA, 8–11 April 2013; pp. 1–12.
21. Arya, M.; Pellegrino, S. Deployment mechanics of highly compacted thin membrane structures. In Proceedings of the Spacecraft Structures Conference, National Harbor, MD, USA, 13–17 January 2014.
22. Sakamoto, H.; Natori, M.C.; Kadonishi, S.; Yasutaka, S.; Shirasawa, Y.; Okuizumi, N.; Mori, O.; Furuya, H.; Okuma, M. Folding patterns of planar gossamer space structures consisting of membranes and booms. *Acta Astronaut.* **2014**, *94*, 34–41. [CrossRef]
23. Guang, C.H.; Yang, Y. Single-vertex multicrease rigid origami with nonzero thickness and its transformation into deployable mechanisms. *J. Mech. Robot.* **2018**, *10*, 011010. [CrossRef]
24. Parque, V.; Suzaki, W.; Miura, S. Packaging of thick membranes using a multi-spiral folding approach: Flat and Curved Surfaces. *Adv. Space Res.* **2020**, *67*, 2589–2612. [CrossRef]
25. Liu, C.J.; Deng, X.W.; Liu, J.; Peng, T.J.; Yang, S.P.; Zheng, Z.L. Dynamic response of saddle membrane structure under hail impact. *Eng. Struct.* **2020**, *214*, 110597. [CrossRef]
26. Gdoutos, E.; Truong, A.; Pedivellano, A.; Royer, F.; Pellegrino, S. Ultralight deployable space structure prototype. In Proceedings of the AIAA Scitech 2020 Forum, Orlando, FL, USA, 6–10 January 2020.
27. Ikeya, K.; Sakamoto, H.; Nakanishi, H.; Furuya, H.; Yamazaki, M. Significance of 3U CubeSat OrigamiSat-1 for space demonstration of multifunctional deployable membrane. *Acta Astronaut.* **2020**, *175*, 363–377. [CrossRef]
28. Okuizumi, N.; Yamamoto, T. Centrifugal deployment of membrane with spiral folding: Experiment and simulation. *J. Space Eng.* **2009**, *2*, 41–50. [CrossRef]
29. Liu, T.; Wang, X.H.; Qiu, X.M.; Zhang, X.H. Theoretical study on the parameter sensitivity over the mechanical states of inflatable membrane antenna. *Aerosp. Sci. Technol.* **2020**, *102*, 105843. [CrossRef]
30. Tessler, A.; Sleight, D.W.; Wang, J.T. Effective modeling and nonlinear shell analysis of thin membranes exhibiting structural wrinkling. *J. Spacecr. Rockets* **2012**, *42*, 287–298. [CrossRef]
31. Liyanage, P.M.; Mallikarachchi, H.M.Y.C. Origami based folding patterns for compact deployable structures. In Proceedings of the 4th International Conference for Structural Engineering and Construction Management, Kandy, Sri Lanka, 13–15 December 2013; pp. 1–13.
32. Satou, Y.; Furuya, H. Local buckling in crease induced by wrapping fold of space membrane. *J. Spacecr. Rockets* **2014**, *51*, 595–603. [CrossRef]
33. Kang, C.W.; Huang, H. FEM stress analysis of interfacial failure of multilayered thin film structures in nanoscratching. *Adv. Mater. Res.* **2016**, *1136*, 289–292. [CrossRef]
34. Cai, J.G.; Ren, Z.; Ding, Y.F.; Deng, X.W.; Xu, Y.X.; Feng, J. Deployment simulation of foldable origami membrane structures. *Aerosp. Sci. Technol.* **2017**, *67*, 343–353. [CrossRef]
35. Wei, J.Z.; Ma, R.Q.; Liu, Y.F.; Yu, J.X.; Eriksson, A.; Tan, H.F. Modal analysis and identification of deployable membrane structures. *Acta Astronaut.* **2018**, *152*, 811–822. [CrossRef]
36. Yuan, T.T.; Liu, Z.Y.; Zhou, Y.H.; Liu, J.Y. Dynamic modeling for foldable origami space membrane structure with contact-impact during deployment. *Multibody Syst. Dyn.* **2020**, *50*, 1–24. [CrossRef]
37. Furuya, H.; Inoue, Y.; Masuoka, T. Deployment characteristics of rotationally skew foldmembrane for spinning solar sail. In Proceedings of the 46th AIAA/ASME/ASCE/AHS/ASC Structures, Structural Dynamics & Materials Conference, Austin, TX, USA, 18–21 April 2006.
38. Zirbel, S.A.; Lang, R.J.; Thomson, M.W.; Sigel, D.A.; Walkemeyer, P.E.; Trease, B.P.; Magleby, S.P.; Howell, L.L. Accommodating thickness in origami-based deployable arrays. *J. Mech. Design.* **2013**, *135*, 111005. [CrossRef]